International Journal of Electronics
Publication details, including instructions for authors and subscription information:
http://www.tandfonline.com/loi/tetn20

New compact dual-band bandstop filter

Anand K. Verma [a], Adel Abdel-Rahman [b], A. Kumar [a], Nainu P. Chaudhari [a], Atallah Balalem [c] & Abbas Omar [c]

[a] Department of Electronic Science, University of Delhi, India

[b] South Valley University, Qena, Egypt

[c] University of Magdeburg, Magdeburg, Germany

Published online: 05 Oct 2012.

To cite this article: Anand K. Verma , Adel Abdel-Rahman , A. Kumar , Nainu P. Chaudhari , Atallah Balalem & Abbas Omar (2013) New compact dual-band bandstop filter, International Journal of Electronics, 100:4, 497-507, DOI: 10.1080/00207217.2012.713020

To link to this article: http://dx.doi.org/10.1080/00207217.2012.713020

International Journal of Electronics, 2013
Vol. 100, No. 4, 497–507, http://dx.doi.org/10.1080/00207217.2012.713020

New compact dual-band bandstop filter

Anand K. Verma[a]*, Adel Abdel-Rahman[b], A. Kumar[a], Nainu P. Chaudhari[a], Atallah Balalem[c] and Abbas Omar[c]

[a]*Department of Electronic Science, University of Delhi, India;* [b]*South Valley University, Qena, Egypt;* [c]*University of Magdeburg, Magdeburg, Germany*

(*Received 1 August 2010; final version received 2 June 2012*)

This article introduces a compact single pole dual-band bandstop filter using capacitors loaded open rectangular DGS slot. A parametric study is reported to pull down lower and upper frequency bands of the unloaded DGS slot in the range of needed stopbands with the help of the loading capacitors. A systematic design process is reported to design a dual-band bandstop filter to suppress 2.4 GHz and 5.2 bands, with bandwidths 0.15/0.25 GHz, by 36 dB and 25 dB respectively. The passband between the two stop-bands has 0.2 dB insertion loss. A circuit model of dual-band bandstop filter is also presented.

Keywords: bandstop filter; dual-band filter; defected ground structure; DGS; filter

1. Introduction

Dual-band bandstop filter (DBSF) is needed at the GSM band to eliminate the interfering signals due to the mobile band. Similarly, we may have to stop the interfering WLAN bands IEEE 802.11 a in the ranges 5.15–5.25 GHz, 5.25–5.35 GHz, 5.47–5.725 GHz, 5.725–5.825 GHz as well as IEEE 802.11b band in the range 2.412–5.484 GHz (Ciampa and Olenewa 2007). Several kinds of dual-band bandstop filters have been introduced in the literature (Woo and Lee 2005; Lee, Oh, and Myung 2006; Tseng and Itoh 2006; Chin, Yeh, and Chao 2007; Lim, Kim, Shin, and Yu 2007; Chao and Qun 2008; Abunjaileh and Hunter 2009; Chin and Lung 2009; Hu 2009; Tang, Hong, and Chun 2009; Kakhki and Neshati 2010; Xiao and Zhu 2011). The coupled short-circuited quarter-wavelength stubs, stepped-impedance stubs, composite right/left handed metamaterial transmission lines, spur-line resonators, defected ground structures (DGS) in the form of the spiral and split ring resonators etc. are used to realise DBSF. The lumped capacitor loaded DGS slot has also been reported to tune the resonant frequency to some extent (Woo and Lee 2005). However, the capacitor loaded DGS slot is not reported in our knowledge to obtain a compact dual-band bandstop filter.

In this article, we propose a new single pole compact dual-band bandstop filter using the lumped capacitors loaded open rectangular DGS slot to suppress the WLAN signals. In the present work we have paid attention to the unlicensed WLAN bands, 2.4 GHz/5.2 GHz. The filter is based on single DGS slot and a new concept of *differential tuning* has been introduced to get two nonharmonically connected stopbands.

*Corresponding author. Email: anandvrm48@gmail.com

The article is organised as follows: Section 2 presents the working process of the proposed dual-band bandstop filter. Section 3 presents the design guidelines to develop the proposed filter on low and high permittivity substrates. It also reports a circuit model of the filter. Section 4 presents the experimental results of the fabricated dual-band bandstop filter to suppress the lower and upper frequency bands of the WLAN. The effect of the package shield on the resonance frequencies is also investigated. Finally, the present DBSF is compared against some of the available DBSF.

2. Working of proposed dual-band single pole band-stop filter

The proposed lumped capacitor loaded open rectangular DGS slot and the electric field distributions on the slot are shown in Figure 1. The slot is etched in the ground plane of a substrate with $\varepsilon_r = 3.38, h = 0.831$ mm. The 50-Ω microstrip line runs, on other side of the substrate, parallel to the arm d_2. The unloaded DGS slot (without lumped capacitors) resonates at two frequencies – the lower band resonance frequency f_L and the upper band resonance frequency f_H, with $f_H/f_L \approx 3$. The simulated $|S_{21}|$ responses of DGS slot, with slot gap $s = 1$ mm, of three different sizes are shown in Figure 2. The lower resonance

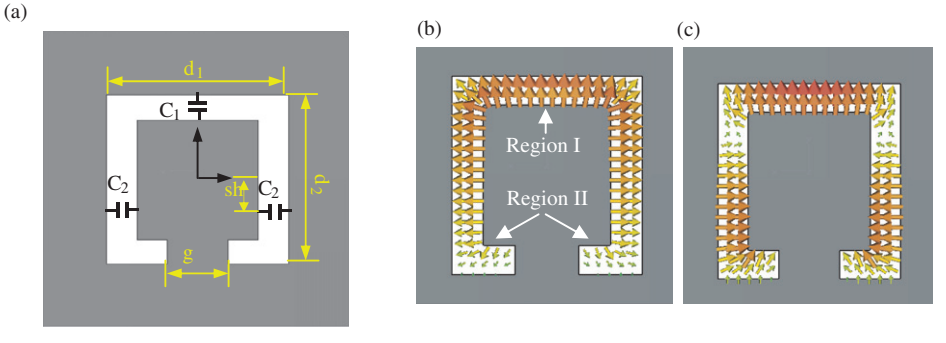

Figure 1. DBSF structure and simulated electric field intensity inside the DGS slot. (a) Bottom side of DGS slot with capacitors; (b) fundamental mode and (c) third harmonic mode.

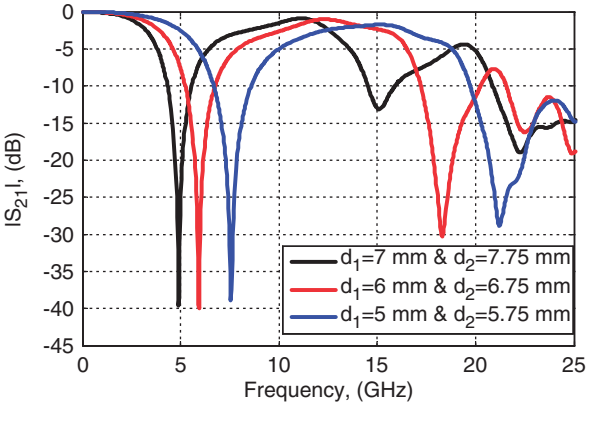

Figure 2. Simulated S_{21} of DGS slot without capacitors.

frequency changes from 4.89 GHz to 5.94 GHz to 7.50 GHz; while the upper resonance frequency increases from 15 GHz to 18.27 GHz to 21.24 GHz on decreasing the size of DGS slot. For the first two larger slots, we have $f_H/f_L \approx 3$. However, for the smaller slot, we have $f_H/f_L = 2.8$. Figure 1(b) and (c) shows the electric field distribution in the slot region at the lower and upper resonant frequencies. At the fundamental resonance frequency, the electric field has one maximum. At the third harmonics, we observe three maxima.

We compute approximate normalised sides d_1, d_2 and slot-width s of the rectangular DGS slot with help of the following curve-fitted empirical expressions:

$$\begin{aligned}
\frac{d_1}{\lambda_g} &= 7 \times 10^{-5}(\lambda_g)^2 - 55 \times 10^{-4}\lambda_g + 0.317 \quad (a)\\
\frac{d_2}{\lambda_g} &= 10^{-4}(\lambda_g)^2 - 86 \times 10^{-4}\lambda_g + 0.4013 \quad (b)\\
\frac{s}{\lambda_g} &= 5 \times 10^{-3}(\lambda_g)^2 - 41.27 \times 10^{-2}\lambda_g + 11.214 \quad (c)\\
\frac{f_H}{f_L} &= -3 \times 10^{-3}(\lambda_g)^2 + 22.59 \times 10^{-2}\lambda_g - 0.3173 \quad (d)
\end{aligned} \tag{1}$$

where the guided wavelength is $\lambda_g = \lambda_0/\sqrt{\varepsilon_r}$. λ_0 is the wavelength corresponding to the lower resonance frequency f_L. The lower resonance frequency f_L is the up-scaled frequency obtained from the specification of the dual-band bandstop filter. The up-scaled upper resonance frequency, f_H is estimated from Equation (1d). As compared to results from the CST EM-simulator (CST Microwave Studio 2008), the lower and upper resonance frequencies can have deviations up to 3% and 15% respectively. However, deviation in resonance frequency is not very important, as the final results get corrected through tuning. We have noted that the lower resonance frequency, f_L is to be scaled down approximately by a factor of 2.5 and the upper resonance frequency, f_H is to be scaled down approximately by a factor of 3.5 to arrive at the needed WLAN stop bands.

2.1. *Differential reduction of lower and upper resonant frequencies with capacitors*

The lumped capacitors connected across the slot regions, shown in Figure 1(a), lower the natural resonance frequencies of the DGS slot in 1–6 GHz band. The capacitors are connected at the locations of the maximum electric field intensity. Through the numerical experimentation on the CST Microwave Studio (2008), we have noted that both f_L and f_H decrease with increasing C_1 and C_2. However, changes in the resonance frequencies are not in same proportion. The *differential change* in frequencies is useful to get *nonharmonically* related two stopband frequencies. Figure 3 illustrates such differential frequency reduction for $C_2 = 0.5$ pF; while C_1 is changed from 0.0 pF to 0.7 pF. There is a large reduction in f_H from 12.5 GHz to 5.21 GHz; whereas only a small variation in f_L from 3.18 GHz to 2.42 GHz. We further noted that the bandwidth of the lower band is not much affected, while for the upper band the bandwidth changes significantly. The larger C_1 provides high Q, i.e. the narrower bandwidths, for both the lower and upper bands; whereas the larger C_2 provides high Q only for the lower band.

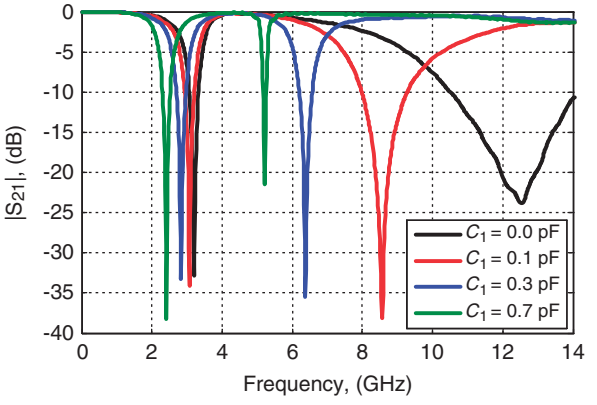

Figure 3. Changes in f_L and f_H for $C_2 = 0.5$ pF and C_1 *is a parameter*.

Table 1. Effect of location (Sh) of C_2 and slot gap (g) resonance frequencies.

Effect of position of C_2						
Position of C_2/slot gap g (mm)	f_L (GHz)	f_H (GHz)	3 dB BW at f_L	3 dB BW at f_H	10 dB BW at f_L	10 dB BW at f_H
2.0	2.08	6.17	0.456	0.466	0.172	0.166
1.0	2.14	5.99	0.472	0.499	0.175	0.180
0.5	2.26	5.60	0.499	0.570	0.186	0.197
0.0	2.34	5.44	0.526	0.585	0.199	0.210
−0.5	2.42	5.29	0.558	0.600	0.205	0.217
−1.5	2.58	5.03	0.632	0.563	0.223	0.208
−2.0	2.67	4.92	0.690	0.541	0.249	0.200
−2.5	2.76	4.85	0.756	0.503	0.267	0.181
Effect of slot gap g						
1	2.26	5.19	0.49	0.64	0.17	0.22
2	2.41	5.20	0.54	0.61	0.20	0.21
3	2.55	5.22	0.60	0.57	0.21	0.20
4	2.68	5.24	0.65	0.54	0.23	0.20

2.2. *Effect of the location (Sh) of the capacitors C_2*

The resonance frequencies are fine tuned in the differential manner by changing the location Sh of two capacitors C_2, shown in Figure 1(a). The electric field distributions shown in Figure 1(b) and (c) suggest that if the locations of the two capacitors C_2 are moved upward, with respect to the centre line, f_L can decrease and f_H can increase. However, if the location of the two C_2 is moved below the centre line, the changes in the resonance frequencies are in opposite directions. Such expected behaviour is shown in Table 1. Table 1 also presents results on 3-dB and 10-dB bandwidths for both bands. These bandwidths are approximately 500 MHz and 200 MHz, respectively. We get nearly constant bandwidths while tuning the bands with the help of the position Sh of capacitors C_2. For the dual-band bandstop filter design, we can fix the upper band accurately by the position of C_2. The correct lower band is obtained by adjusting the slot gap g.

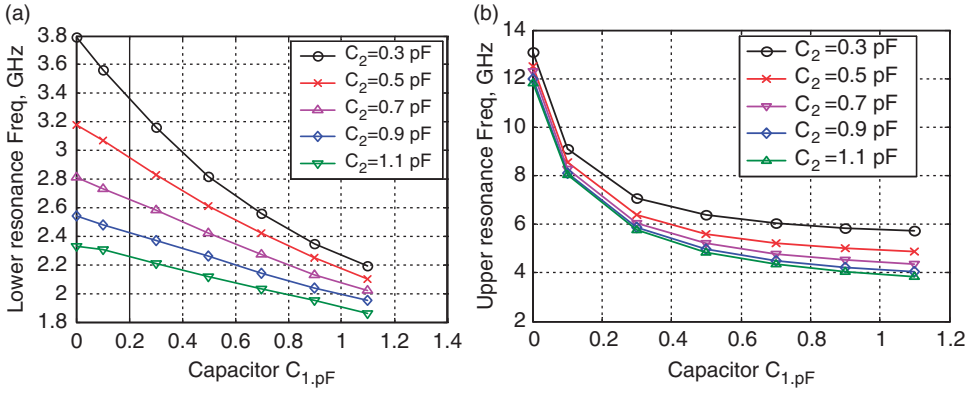

Figure 4. Design graphs for computing C_1 and C_2. (a): Known lower band frequency, f_L; (b) Known upper band frequency, f_H.

2.3. *Effect of the slot-gap (g)*

Our investigation on CST EM-simulator (CST Microwave Studio 2008) has further shown that f_L decreases on decreasing the slot-gap g. However, it has insignificant effect on f_H. These findings are shown Table 1. Therefore, g could be selected to get the lower IEEE 802.11b band without disturbing the upper IEEE 802.11a band determined by the location of C_2. Table 1 further shows that the bandwidths of lower bands decrease a little, while for the upper band the bandwidths increase a little, for a narrower slot-gap.

3. Design of dual-band bandstop filter and circuit model

The capacitors C_1 and C_2 are selected with the help of the design graphs shown in Figure 4. Figure 4(a) and (b) show the variation in f_L and f_H with respect to the capacitor C_1, while capacitor C_2 is a parameter. The differential variation in both resonance frequencies is obvious for the identical variation in the capacitance. Figure 4(a) is used to obtain the values of capacitors C_1 and C_2 from the lower band frequency f_L, which is known from specification of the filter. The values of C_1 and C_2 should also satisfy specification on the higher band rejection frequency f_H shown in Figure 4(b).The combination of C_1 and C_2 are selected for sharp high-Q resonances. For various combinations, sharp high-Q resonances are tested on the EM-simulator. The graphical design of DBSF is illustrated for three cases – case #1, 2.4/5.2 GHz and case #2, 2.0/4.1 GHz and case #3, 2.4/5.2 GHz. First, the filters are designed on substrate with $\varepsilon_r = 3.38, h = 0.831$ mm. In order to establish confidence in the design process, the third filter is designed on substrate with $\varepsilon_r = 10.2$, $h = 0.831$ mm. The design steps are as follows:

First, we compute the size of the DGS slot from the lower frequency of the DBSF. For case #1, 2.4/5.2 GHz band, we up-scale the lower frequency by a factor of 2.5 and compute the size of the slot with help of Equations (1a)–(c). We also estimate the up-scaled upper frequency by Equation (1d). The computed DGS slot in 50 Ω microstrip is simulated on the EM-simulator to get two correct sharp resonances. Figure 5(a) shows both up-scaled resonance frequencies. We may have to tune the slot size a bit to get sharp resonances.

Next, we pull down both lower and upper band frequencies with the help of the capacitors C_2 and C_1 in the range of the required two bands. For this purpose we mark 2.4 GHz on the vertical frequency axis of Figure 4(a) and draw a line parallel to the horizontal C_1 axis. We get three pairs of solutions for (C_1, C_2) in pF as (0.3, 0.9), (0.5, 0.7) and (0.7, 0.5). The values of (C_1, C_2) should also provide 5.2 GHz from Figure 4(b).The values of (C_1, C_2) should also provide high-Q sharp resonances for both the lower and upper bands. To meet these requirements, we select value (0.5, 0.7) pF for (C_1, C_2). It provides approximate resonances 2.36/5.06 GHz, in the needed bands. The results are shown in Figure 5(b).

Finally, using the EM-simulator, the correct upper band frequency is obtained at 5.2 GHz by locating two C_2 capacitors at Sh = −0.5 mm below the centre line. The slot-gap g is adjusted at 3 mm to get the correct lower band frequency. Sometimes, on selecting the slot-gap g to fix the needed lower band frequency f_L, there may be some shifting in the upper band frequency f_H. The correct f_H can be obtained by relocating the position of two capacitors C_2.

For case #2, we get (C_1, C_2) as (1, 0.9) pF. Figure 6(a) shows 1.93/4.02 GHz resonances. For C_2 location (Sh = 0 mm) and slot-gap (g = 2 mm), we finally obtain the needed 2.0/4.1 GHz bands. Likewise, for the case #3, using the substrate $\varepsilon_r = 10.2$, $h = 0.831$ mm, we get slot dimensions $d_1 = 3.88$ mm, $d_2 = 4.56$, $s = 1$ mm, for the up-scaled frequencies 6/14.9 GHz. Final 2.4/5.2 GHz rejections are obtained for $C_1 = 0.4$ pF, $C_2 = 0.7$ pF $g = 1.5$ mm, Sh = +0.5 mm. Figure 6(b) shows the simulated results.

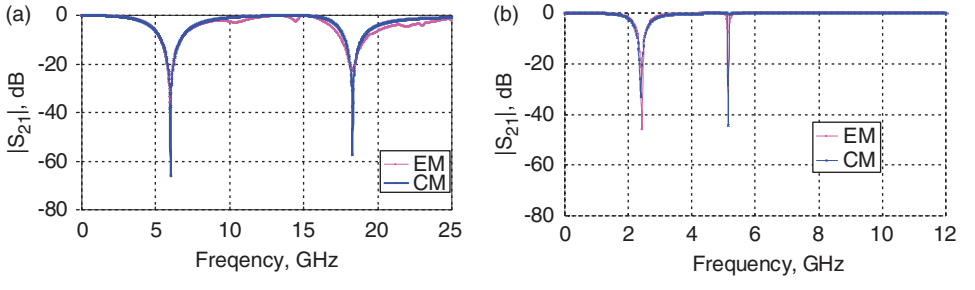

Figure 5. Up-scaled and down-scaled (2.4/5.2 GHz) resonance frequencies using EM-simulator (EM) and Circuit model (CM). (a) Up-scaled resonance frequencies of DBSF; (b) 2.4/5.2 GHz DBSF ($C_1 = 0.5$ pF, $C_2 = 0.7$ pF). Substrate: $\varepsilon_r = 3.38$, $h = 0.831$ mm.

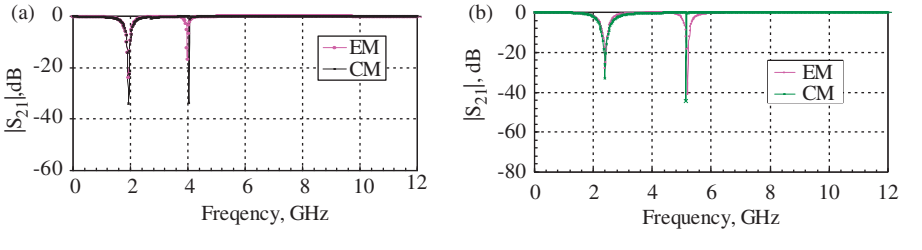

Figure 6. EM simulator (EM) and circuit model (CM) response for 2.4/5.2 GHz and 1.93/4.02 GHz filter filters. (a): 1.93/4.02 GHz DBSF, ($C_1 = 0.1$ pF, $C_2 = 0.9$ pF $\varepsilon_r = 10.2$, $h = 0.831$ mm; (b) 2.4/5.2 GHz DBSF, ($C_1 = 0.4$ pF, $C_2 = 0.7$ pF), $\varepsilon_r = 3.38$, $h = 0.831$ mm.

Figure 7(a) and (b) show the circuit models of the present dual-band bandstop filters without capacitors and with loading capacitors respectively. The component values (C_L, L_L) and (C_H, L_H) for lower and upper frequencies, respectively, are obtained from the following expression (Abdel-Rahman, Verma, Boutejdar, and Omar 2004):

$$C_k = \frac{5f_{c,k}}{\pi\left(f_{0,k}^2 - f_{c,k}^2\right)} pF \quad (a), \quad L_k = \frac{250}{C_k\left(\pi f_{0,k}\right)^2} nH \quad (b), \quad \text{where } k = L, H \tag{2}$$

Normally, the above expressions are used for the single resonance. However, we have adopted it for dual resonances. Thus $f_{0,k}$ is the pole frequency of both the lower (f_L) and upper (f_H) resonances and $f_{c,k}$ is the 3 dB cut-off frequency associated with both the resonances.

Once the DGS slot is loaded with capacitors, both resonance frequencies are reduced. We have to add shunt capacitors C_1 and C_3 with resonators as shown in Figure 7(b). However, addition of the parallel capacitors also disturbs the fields in the slot region. It is accounted for by introducing the coupling capacitor C_2'in the model. In Figure 7(b) C_1 is the loading capacitor and the capacitors $C_2'$and C_3 are related to another loading capacitor C_2 as follows:

$$\begin{aligned} C_2' &= 2C_2 \quad (a) \\ C_3 &\approx 7C_2' \quad (b) \end{aligned} \tag{3}$$

Table 2 shows the values of these capacitors for three cases. Figures 5 and 6 compare the accuracy of the circuit model for three cases against the results of the EM-simulator. The results from both the sources are almost identical.

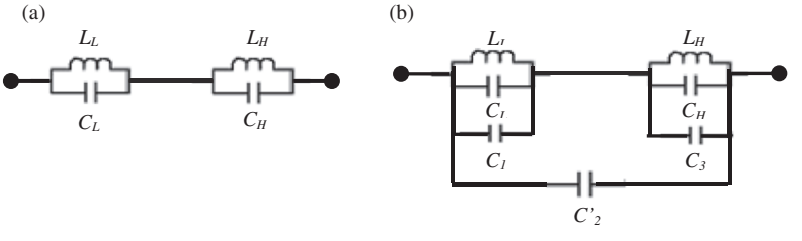

Figure 7. Circuit models of unloaded and capacitors loaded dual-band bandstop filter. (a) Unloaded dual-band DGS slot; (b) capacitors loaded dual-band DGS slot.

Table 2. Element values of the circuit model for three cases.

Cases	C_1 pF	C_3 pF	$C_2' = 2C_2$ pF	f_L (GHz)	f_H (GHz)
1	0.50	4.83	1.44	2.41	5.20
2	0.90	8.51	1.90	2.42	5.22
3	0.45	4.97	0.90	2.575	5.75

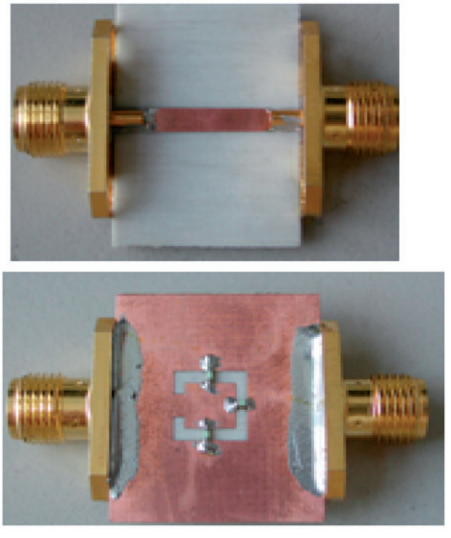

Figure 8. Photographs of top and bottom views of the fabricated filter.

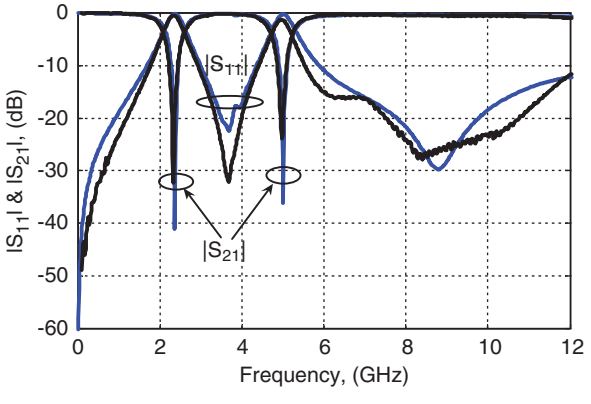

Figure 9. Measured (solid) and simulated (dashed) response of the dual band filter.

Table 3. Effect of back shield on resonance frequencies.

H (mm)	f_L (GHz)	f_H(GHz)
1	2.400	5.195
2	2.364	5.172
3	2.353	5.166
4	2.331	5.161
No back shield	2.320	5.15

Table 4. Effect of slot width on 3 dB bandwidth and Q.

Slot width s (mm)	3 dB BW at f_L (GHz)	3 dB BW at f_H (GHz)	10 dB BW at f_L(GHz)	10 dB BW at f_H (GHz)	Q –Factor at f_L	Q –Factor at f_H	Attenuation (dB/GHz)		Sharpness (dB/GHz)	
							at f_L	at f_H	at f_L	at f_H
0.5	0.29	0.17	0.18	0.09	8.5	28.47	22.7	29.5	62.96	212.5
1.0	0.15	0.25	0.12	0.09	16	22.22	25	36	62.96	340.0
1.5	0.40	0.19	0.15	0.08	6.12	30.52	30.2	27.8	58.62	212.5

Table 5. Comparison of our filter against available DBSF.

Ref No.	Lower/upper resonance freq. (GHz)	Lower/upper 3 dB BW (GHz)	Lower/upper Q_L/Q_U	I.L. (dB)	Attenuation at f_L/f_U (dB)	Area (mm^2)
Woo and Lee 2005	3.00/4.50	0.60/0.35	5.0/12.85	0.9	18/15	24.96
Chin et al. 2007	1.57/3.16	0.84/0.76	1.87/4.16	0.9	46/45	666.4
Xiao and Zhu 2011	1.89/5.69	0.69/0.55	2.74/10.35	0.7	26/14	36.00
Attaran Kakhki and Neshati 2011	4.02/5.12	0.69/0.46	5.83/11.14	0.5	34/34	36.00
Hu 2009	2.52/5.35	0.28/0.10	9.14/53.50	0.8	33/16	39.06
Chin and Lung 2009	2.35/5.58	0.97/1.00	2.42/5.580	0.6	45/38	1600
Ours	2.40/5.20	0.15/0.25	16.0/22.00	0.2	35/25	40.50

4. Fabrication and experimental results of proposed dual-band

4.1. *Bandstop filter*

The DBSF of case #1 suppresses the WLAN IEEE 802.11 a/b bands. The filter dimensions are $d_1 = 6$ mm, $d_2 = 6.75$ mm, $g = 2$ mm, and the slot width is 1 mm. The loading capacitors are $C_1 = 0.5$ pF and $C_2 = 0.7$ pF. The filter is simulated, fabricated and measured. Figure 8 shows the photographs of the fabricated structure. Figure 9 shows the simulated and measured results of the filter. The simulated lower and upper bands are 2.37 GHz and 5.19 GHz; while the measured ones are 2.32 GHz and 5.15 GHz. The simulated lower and upper band rejections are 41 dB and 32 dB, respectively; whereas the measured lower and upper bands rejections are better than 36 dB and 25 dB, respectively. The measured insertion loss, between the two stopbands, is 0.2 dB.

From the packaging point of view, we have further examined experimentally the effect of back shield, facing the slot, on both the resonance frequencies. The back shield also controls the radiation from the slot. The results are summarised in Table 3. We note only a small change, 100 MHz and 45 MHz, in f_L and f_H, respectively. For the shield height (H) above 6 mm there is no change in the resonance frequencies. We have also noted that bandwidths are nearly unchanged. The position of the shield can be used to tune both the frequency within 100 MHz and 45 MHz for f_L and f_H, respectively. In the present design, the intended WLAN bands – 2.4 GHz/5.2 GHz are achieved by the use of the shield at 1 mm from the substrate. However, Table 4 further examines the effect of the slot-width s on bandwidths and loaded Q-factors. We note that the slot width could be used to control the bandwidth loaded Q-factor, rejection attenuation and sharpness of both resonances. However, 1.0 mm slot-width is a satisfactory choice. It is further confirmed by comparison of performances of our DBSF against some of the available filters as shown in Table 5. Our compact filter has better performance in respect of insertion loss (IL), simultaneous high rejection for both bands and their high Q-factors. The filter of Chin and Lung (2009) has better rejections; but the size of filter is large.

5. Conclusion

A single pole compact dual-band bandstop filter using the capacitor loaded DGS slot is presented. The design is based on a new concept of differential tuning to get two nonharmonically connected stopbands. A systematic graphical design process of a dual-

band bandstop filter is given that is applicable to both the low and high permittivity substrates. The stopbands 2.32 GHz and 5.15 GHz are suppressed by 36 dB and 25 dB, respectively, with 0.2 dB insertion loss for the passband between the two stopbands. A circuit model for the dual-band bandstop filter is also presented.

Acknowledgement

Prof. A. K.Verma is thankful to UGC for the project grant. The authors are thankful to reviewers for their suggestions.

References

Abdel-Rahman, A.B., Verma, A.K., Boutejdar, A., and Omar, A.S. (2004), 'Control of Bandstop Response of Hi-lo Microstrip Low-pass Filter using Slot in Ground Plane', *IEEE Transaction on Microwave Theory and Techniques*, 52, 1008–1013.

Abunjaileh, A.I., and Hunter, I.C. (2009), 'Tunable Combline Bandstop Filter with Constant Bandwidth', in *2009 IEEE MTT-S International Microwave Symposium Digest*, 7–12 June, USA, pp. 1611–1614.

Attaran Kakhki, M., and Neshati, M.H. (2010), 'Novel Dual Band-reject DGS Filter with Improved Q Factor' in *Ist International Conference on Communications Engineering,* 22–24 December, University of Sistan & Baluchestan, pp. 73–86.

Chao, C., and Qun, W. (2008), 'A Novel Spurline Bandstop Filter Using Defected Ground and Defected Microstrip Structures', in *Microwave Conference*, China-Japan Joint, 10–12 September, pp. 75–77.

Chin, K.S., and Lung, C.K. (2009), 'Miniaturized Microstrip Dual-bands Stop Filters Using Tri-section Stepped-impedance Resonators', *Progress in Electromagnetics Research C*, 10, 37–48.

Chin, K.-S., Yeh, J.-H., and Chao, S.-H. (2007), 'Compact Dual-band Bandstop Filters Using Stepped-impedance Resonators', *IEEE Microwave & Wireless Components Letters*, 17, 849–851.

Ciampa, M., and Olenewa, J. (2007), *Wireless Communications, Course Technology*, Singapore: Cengage Learning.

CST Microwave Studio (2008), www.cst.com.

Hu, X. (2009), 'Compact Dual-band Rejection Filter Based on Complementary Meander Line Spilt Ring Resonator', *Progress in Electromagnetics Research Letters*, 8, 181–190.

Lee, J.H., Oh, Y.C., and Myung, N.H. (2006), 'A Novel Compact Microstrip Bandstop Filter Based on Complementary Split-ring Resonators', in *Asia Pacific Microwave, Conference (APMC2006)*, 12–15 December, Yokohama, Japan.

Lim, W.G., Kim, W.K., Shin D.H., and Yu, J.W. (2007), 'A Novel Bandstop Filter Design Using Parallel Coupled Line Resonators', in *European Microwave Conference*, 9–12 October, pp. 878–881.

Tang, W., Hong, J.S., and Chun, Y.H. (2009), 'Microstrip Cross-coupled Stepped-impedance Line Bandstop Filter', in *2009 IEEE MTT-S International Microwave Symposium Digest*, 7–12 June, USA, pp. 645–648.

Tseng, C.H., and Itoh, T. (2006), 'Dual-band Bandpass and Bandstop Filters Using Composite Right/Left-handed Metamaterial Transmission Lines', in *Microwave Symposium Digest*, 11–16 June.

Woo, D.-J., and Lee, T.-K. (2005), 'Suppression of Armonics in Wilkinson Power Divider Using Dual-band Rejection by Asymmetric DGS', *IEEE Transactions on Microwave Theory and Techniques*, 53, 2139–2144.

Xiao, J.-K., and Zhu, W.-J. (2011), 'New Defected Microstrip Structure Bandstop Filter', *Progress in Electromagnetics Research Symposium Proceedings*, 12–16 September, Suzhou, China, pp. 1471–1474.